Journal of Computational Neuroscience (2019) 47:1–16
https://doi.org/10.1007/s10827-019-00714-8

Slow-gamma frequencies are optimally guarded against effects of neurodegenerative diseases and traumatic brain injuries

Pedro D. Maia[1,2] · **Ashish Raj**[1,2] · **J. Nathan Kutz**[3]

Received: 17 August 2018 / Revised: 2 February 2019 / Accepted: 19 March 2019 / Published online: 4 June 2019

Abstract

We introduce a computational model for the cellular level effects of firing rate filtering due to the major forms of neuronal injury, including demyelination and axonal swellings. Based upon experimental and computational observations, we posit simple phenomenological input/output rules describing spike train distortions and demonstrate that slow-gamma frequencies in the 38–41 Hz range emerge as the most robust to injury. Our signal-processing model allows us to derive firing rate filters at the cellular level for impaired neural activity with minimal assumptions. Specifically, we model eight experimentally observed spike train transformations by discrete-time filters, including those associated with increasing refractoriness and intermittent blockage. Continuous counterparts for the filters are also obtained by approximating neuronal firing rates from spike trains convolved with causal and Gaussian kernels. The proposed signal processing framework, which is robust to model parameter calibration, is an abstraction of the major cellular-level pathologies associated with neurodegenerative diseases and traumatic brain injuries that affect spike train propagation and impair neuronal network functionality. Our filters are well aligned with the spectrum of dynamic memory fields including working memory, visual consciousness, and other higher cognitive functions that operate in a frequency band that is - at a single cell level - optimally guarded against common types of pathological effects. In contrast, higher-frequency neural encoding, such as is observed with short-term memory, are susceptible to neurodegeneration and injury.

Keywords Slow-gamma · Neurodegenerative disease · Alzheimer · Traumatic brain injury · Focal axonal swelling · Demyelination · Spike-train robustness

Action Editor: Ingo Bojak

Electronic supplementary material The online version of this article (https://doi.org/10.1007/s10827-019-00714-8) contains supplementary material, which is available to authorized users.

✉ Pedro D. Maia
pedro.doria.maia@gmail.com

Ashish Raj
asr2004@med.cornell.edu

J. Nathan Kutz
kutz@uw.edu

[1] Weill Cornell Medicine, Department of Radiology, New York, NY, USA

[2] Weill Cornell Medicine, Brain and Mind Research Institute, New York, NY, USA

[3] Department of Applied Mathematics, University of Washington, Seattle, WA 98195-2420 USA

1 Introduction

Spike trains are the fundamental electrical units for signal transmission and information processing in neural systems. Although the exact information content encoded in spike trains remains a grand challenge problem in neuroscience, compromised spike trains are known to produce deleterious effects on neurological and neuro-sensory function. Indeed, neurodegenerative diseases and traumatic brain injuries produce a host of axonal level pathologies that deteriorate spike train propagation, resulting in cognitive deficits and reduced neural function.

Axonal damage is commonly produced by either demyelination and/or focused axonal swelling (FAS) of the neuron, thus leading to spike train transformations whereby some or all spikes in a spike train are deleted and/or delayed. These transformations, verified by experiments (Smith 1994), can be characterized by classical cable equation models for spike train propagation (Maia and Kutz 2017,

2014a, b; Maia et al. 2015). Based upon these self consistent experimental and computational observations, we posit simple phenomenological input/output rules describing spike train distortions. This leads us to develop a general signal processing model whereby the spike train distortions act as filters for firing rate neural activity. The minimal, and experimentally backed, assumptions show that the slow-gamma frequencies in the 38–41 Hz range emerge as the most robust to injury, thus having significant implications for the optimal, from the viewpoint of injury, encoding of neuronal activity. Our model, which is robust to model parametrization, provides the first quantitative assessment of the effects of injury and its relationship to critical frequencies implicated in cognitive function. It further provides new insights into the cognitive deficits that arise in common brain disorders due to the axonal injuries implicated in Alzheimer's Disease (AD), Multiple Sclerosis (MS), and Traumatic Brain Injury (TBI), for instance.

A common practice in computational neuroscience is to model neuronal pathologies in a binary way, by treating a neuron and/or its connections as either fully functional or fully impaired. Recent developments show, however, that these simple strategies cannot capture frequency-dependent errors in spike-train propagation that arise in leading brain disorders. Axonal injury in absence of frank cell death can be classified into two broad classes: axonal swelling and demyelination. Neither injury can be properly captured using a binary approach. Thus their effects on downstream neuronal activity and impairment must be more accurately modeled. Using experimental observations and computational studies, we properly account for the degraded neural activity by building filter models for the firing rate activity.Specifically, we develop a simple model of how these two kinds of axonal injury affect frequency-dependent signal transmission and impair neural activity at a single-cell level.

Neurodegenerative diseases and TBI are prevalent in society. TBI in particular is a serious threat to youngsters, soldiers and contact-sport practitioners across the globe that can lead to persistent functional deficits, disability, and even death. TBI pathologies span several spatial scales, from cellular levels (Browne et al. 2011; Dikranian et al. 2008; Wang et al. 2011) to tissue (Jorge et al. 2012) and network levels (Sharp et al. 2014). As recently summarized in Maia and Kutz (2017), one ubiquitous TBI signature at the cellular level is the presence of swellings along axonal tracts (also referred to as varicosities, spheroids, bulbs or beads) (Edlow et al. 2016; Johnson et al. 2013; Hanell et al. 2015; Henninger et al. 2016; Hill et al. 2016; Morrison et al. 2011; Reeves et al. 2012). Focal Axonal Swellings (FAS) were reported in TBI studies *in vivo* (Browne et al. 2011; Dikranian et al. 2008; Wang et al. 2011) , *in vitro* (Hellman et al. 2010; Hemphill et al. 2015; Magdesian et al. 2012; Tang-Schomer et al. 2010, 2012), and in human patients (Adams et al. 2011; Jorge et al. 2012). FAS gained significant attention from the broader biomedical and neuroscience community because they are also present in brain disorders such as AD (Adalbert et al. 2009; Daianu et al. 2016; Krstic and Knuesel 2012), MS (Friese et al. 2014; Nikic et al. 2011; Trapp and Nave 2008), Parkinson's Disease (Tagliaferro and Burke 2016; Louis et al. 2009) and others (Herwerth et al. 2016; Karlsson et al. 2016; Laukka et al. 2016). More recently, computational models investigated the effects of FAS on spike train propagation (Kolaric et al. 2013; Lachance et al. 2014; Maia et al. 2015; Maia and Kutz 2014a, b) and the functional impairments they cause collectively at a network level (Maia and Kutz 2017; Rudy et al. 2016).

The effects of FAS on spike conduction are similar to those observed after demyelination (Smith 1994; Zlochiver 2010; Verden and Macklin 2016), which play a major role in MS (De Stefano et al. 1995; Trapp et al. 1998; Kornek et al. 2000). We depict both forms of injury in Fig. 1a–b. Figure 1c shows different types of spike-train distortions summarized by Smith (1994) such as conduction block, spike velocity reduction, refractory-period prolongation, refractoriness accumulation, intermittent blockage, and spike evocation. Figure 1d shows similar effects caused by FAS, adapted from Maia and Kutz (2017, 2015, 2014a, b).

We model the distorted neural encodings of neurons impaired under axonal injury and/or demyelination, thus allowing us to understand and predict the likely functional deficits resulting from a variety of disorders. Our goal is to express these models in terms of a signal processing framework where continuous and discrete-time filters capture the input/output relationships of impaired neural connections as a function of frequency, spanning the entire range of neural activity observed from modern recording techniques. Such frequency-resolved models are not currently available in the field. Our main result is that slow-gamma rhythms (25–50 Hz) are surprisingly well-preserved and optimally guarded against the most common type of spike-train distortion, while high frequencies are severely exposed to it. The most robust frequency remains in the specific range of 38–41 Hz independent of our parameter and methodological choices. This may provide a compelling explanation as to why this frequency range is involved in so many higher cognitive functionalities and in visual consciousness.

2 Results

We derive simple input/output (i/o) rules at the cellular level that transform healthy neuronal spike train responses into injured ones, with filters that can be either discrete-time

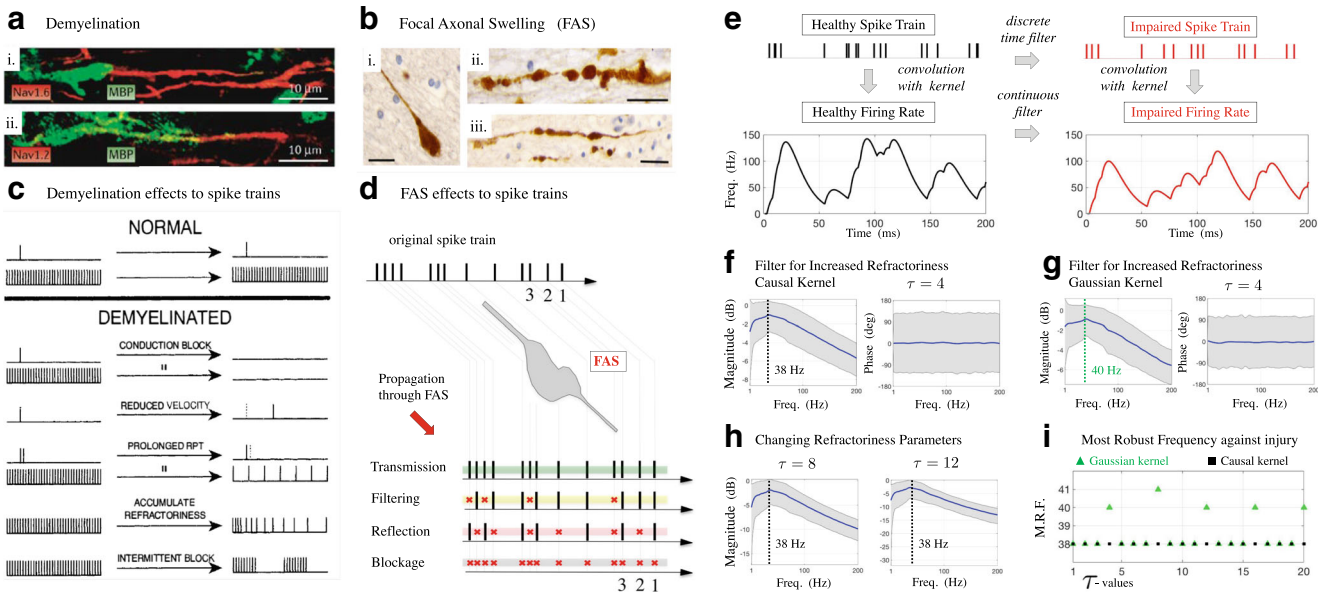

Fig. 1 **a** Multiple Sclerosis (MS) lesions in spinal cord tissue, in which axons display residual damaged myelin (green), adapted from S. Waxman (Waxman 2006). Demyelination is the dominant pathology in MS. **b** Axonal pathology in the form of varicosities (FAS) in the corpus callosum of a young male who died 10h following traumatic brain injury (TBI). Adapted from Johnson et al. (Johnson et al. 2013); scale bars of 15m (i) and 30m (ii-iii). FAS is a ubiquitous pathological feature of TBI across all severities. **c** Schematic representation of the conduction properties of normal vs demyelinated central axons, adapted from K. Smith (Smith 1994). Note that demyelination may significantly distort the original spike trains, and consequently, the information encoded in them. **d** Schematics for FAS effects to spike trains, adapted from Maia and Kutz (Maia and Kutz 2017). A–D: In this work, we develop a simple mathematical framework to describe the anomalous changes that spike trains undergo with discrete and continuous filters for neuronal activity. Note that in all cases, higher frequencies are typically more affected than lower ones. **e** Schematics for frequency-dependent filters for neuronal impairments. Healthy spike trains are transformed into impaired spike trains via discrete-time filters given by i/o rules. Firing-Rate (FR) responses are analogously transformed via continuous-time filters. Spike trains may be converted into FR signals by convolving them with kernels (typically gaussian or causal). **f** Frequency dependent filter (bode plots) for increased refractoriness, the most important type of axonal injury. The Most Robust Frequency (MRF) to injury is 38 Hz when causal kernel and $\tau = 4$ are used. **g** Analogous bode plots using gaussian kernel yields MRF = 40 Hz. **h** Changing the refractory parameter does not affect the qualitative shape of the filter. **i** MRF remains in the 38–41 Hz frequency range independently of parameter and kernel choices

(for spike trains) or continuous-time (for firing rates) signal processors. See Fig. 1e for a simple schematic. Recall that these transformations, verified by experiments (Smith 1994), can be characterized by classical cable equation models for spike train propagation (Maia and Kutz 2017; Maia et al. 2015; Maia and Kutz 2014a, b). Thus our analysis merges standard methods from computational neuroscience with an extensive literature in neurology. Specifically, there are eight characteristic transformations of a spike train which we account for.

2.1 Frequency-dependent filters for neuronal impairments

We assume that a spike train $\{x_n\}$ is transformed into another spike train $\{y_n\}$ according to some rule H :

$$\underbrace{[x_0, x_1, \ldots, x_n]}_{original} \xrightarrow{H} \underbrace{[y_0, y_1, \ldots, y_n]}_{impaired}$$

We treat an impairment as a rule that specifies how to compute the output sequence from the knowledge of the input sequence $\{x_n\}$. For simplicity, entries are either 1 (for a spike) or 0 (else wise), and are typically processed one at a time by a state machine. The eight i/o rules below detail the assumptions in our model, with the first two rules corresponding to mild and severe injury respectively.

(i) *Normal conduction* If faithful conduction occurs, the entries of the input/output spike trains will match:

$$y_n = 1 \cdot x_n \tag{1}$$

This is expected in the case of mild injury.

(ii) *Total blocking* In the case of severe injury, potentially leading to an axontotomy, the axonal impairment will delete all spikes in the train so that:

$$y_n = 0 \cdot x_n \tag{2}$$

(iii) *Reducing spike velocity* Delaying the entire spike train by k time units yields a relatively straightforward rule:

$$y_n = x_{n-k} \tag{3}$$

(iv) *Increasing spike velocity* Anticipating the entire spike train by k time units yields an analogous expression:

$$y_n = x_{n+k} \tag{4}$$

(v) *Increasing refractoriness* This rule will be discussed extensively throughout this work:

$$y_n = x_n - \delta(y_{n-j} + x_n - 2) \text{ for } j = 1, \ldots, \tau \tag{5}$$

where δ refers to the kronecker delta

$$\delta(i) = \begin{cases} 1 \text{ if } i = 0, \\ 0 \text{ otherwise,} \end{cases}$$

and τ is the new (increased) refractory period induced by the i/o rule. This mathematical formulation incorporates the *conditional* aspect of the spike deletion. For example, let $x = [1, 1]$ and $\tau = 1$, then $x_1 = 1, x_2 = 1$ and $y_1 = 1$ (by convention). However:

$$\begin{aligned} y_2 &= x_2 - \delta(y_1 + x_2 - 2) \\ &= 1 - \delta(1 + 1 - 2) \\ &= 1 - 1 = 0. \end{aligned}$$

Thus, if $x = [1, 1]$ then $y = [1, 0]$. It is easy to verify that under this rule, $[1, 0] \rightarrow [1, 0]$ and $[0, 1] \rightarrow [0, 1]$. Equation (5), when applied successively, generalizes this to an arbitrary Inter-Spike Interval (ISI) of length j, giving:

$$[\underbrace{1, 0, 0, \ldots, 0, \mathbf{1}}_{j}] \rightarrow [\underbrace{1, 0, 0, \ldots, 0, \mathbf{0}}_{j}].$$

This impairment is frequency-dependent; spike trains with higher firing rates (and consequently, with shorter ISI) are more strongly affected than spike trains with lower firing rates. This will ultimately lead to confusions of higher firing rates by lower ones. Figure 1e exemplifies this rule to a Poisson spike train. We also derive continuous, firing-rate (frequency) signals for both healthy/impaired spike trains by convolving them with a Gaussian or causal kernel (see SI). Figure 1f–g show continuous counterparts (filter bode-plots) for the i/o rule above.

(vi) *Accumulating refractoriness* This type of impairment is a variant of the previous case, where the new refractory period τ induced by the i/o rule changes over time according to some function. A few examples include:

$$\tau(n) = \begin{cases} linear\,(n), & \text{leading to total blocking,} \\ sigmoid\,(n), & \text{leading to a steady value,} \\ sawtooth\,(n), & \text{reseting } \tau \text{ periodically.} \end{cases} \tag{6}$$

(vii) *Intermittent blocking* In this case, the impairment switches between (total) blocking and normal conduction over time. This can be achieved by multiplying x_n by either 0 or 1 (at every time n) accordingly. If the regimes switch periodically with a duration of $2\pi/\omega$, we can write the i/o rule concisely as:

$$y_n = x_n \cdot square\,(n, \omega) \tag{7}$$

where $square\,(n, \omega) = \frac{1}{2}\,(sign\,[\sin(\omega \cdot n)] + 1)$ is a wave function alternating between 0 and 1 with frequency ω. See Fig. 3 for an illustrative example. There, the top plot exemplifies a healthy Poisson spike train (in black) and the corresponding injured spike train (in red). Notice that injured spike train exhibit periodic windows of no firing activity. The additional plots in Fig. 3 approximate the firing rates of both spike trains by convolving them with commonly used kernels.

(viii) *Evoking potentials* This rule is used when a single input spike triggers the formation of k additional spikes:

$$y_n = \max\{x_n, x_{n-1}, \ldots, x_{n-k}\} \tag{8}$$

For e.g., let $k = 2$, and $x = [0, 0, 1, 0, 0, 0]$. Then, we have $y_3 = \max\{0, 0, 1\}$, $y_4 = \max\{0, 1, 0\}$, and $y_5 = \max\{0, 0, 1\}$, but $y_6 = max\{0, 0, 0\}$. Thus, $y = [0, 0, 1, 1, 1, 0]$, with the single spike in the input train evoking $k = 2$ following spikes. Equation (8) generalizes this example to k evoked spikes, giving:

$$[\,0, 0, 1, \underbrace{0, 0, \ldots, 0}_{k}, 0, 0\,] \rightarrow [\,0, 0, 1, \underbrace{1, 1, \ldots, 1}_{k}, 0, 0\,].$$

This type of impairment is also frequency-dependent, but it affects sparser spike trains more strongly. In fact, dense spike trains already have too many spikes and the addition of evoked spikes does not significantly alter its frequency. Lower firing rates, on the other hand, are more easily confused with higher ones proportionally to k.

By convolving the spike-trains with appropriate kernels (window functions) before and after injury, we can obtain firing-rate counterparts for rules (i)-(viii). See Section 4.5 for details on how we estimated continuous transfer functions for impairments.

2.2 Frequencies near 38–40 Hz are optimally guarded against injury

Figure 1f–i show that regardless of or kernel choice, the magnitude bode-plots always have the same qualitative shape, each with a clear Most Robust Frequency (MRF). More importantly, as shown in Fig. 1i, the MRF remains in the 38–41 Hz range independently of parameter and kernel choices (see the SI for a detailed discussion of parameter sensitivity testing). Thus our results demonstrate the emergent robustness property of cells at slow gamma frequencies.

Robustness of hippocampal slow band in memory retrieval It has been suggested that the gamma band signal can be broken into 3 distinct bands – slow, medium and fast, each with likely a different mechanism of signal generation (Browne et al. 2011). Therefore one of the implications of our work will be that these bands would be subject to differential degradation effects due to axonal injury, since our model shows that slow gamma (35-50Hz) will be better preserved than the higher ones. This would further imply that memory retrieval (a function of low gamma between CA3 and CA1, see Colgin et al. (2009)) should not be as affected in such injuries as memory formation (function of high gamma in CA1, from Colgin et al. (2009)). As we note below, this is indeed the case in TBI and other axonal injuries.

Colgin et al. (2009) showed that the neural circuits of the CA1 area of the hippocampus (known for its critical role in memory) support two distinguished bands of gamma oscillations: a fast band (≈ 90 Hz) and a slow band (≈ 40 Hz). Figure 2a shows a cross-frequency coherence plot showing the two separate bands (fast and slow) of gamma power (y-axis) modulated by the theta phase (x-axis) as the rats explore a familiar environment. The coupling strength is color-coded (dark blue, no coupling; red, maximal coupling). Figure 2b shows time-frequency representations of power for a representative recording, averaged across (a) all theta cycles and (b) theta cycles with slow-gamma (Colgin et al. 2009). Both panels clearly illustrate the split of gamma oscillations into two ranges. While it is expected that the hippocampus should operate within different gamma ranges for different modalities, it is not clear why these particular values are used. Figure 1 suggests a compelling hypothesis, namely, that slow-gamma frequencies are used to overlap with the MRF range of 38-41 Hz. Thus, slow-gamma frequencies are optimally guarded at a cellular level against common types of spike-train anomalies while the faster bands are not.

Injury filter aligns with spectrum of working memory Pesaran et al. (2002) point out the preference for slow-gamma ranges in working memory tasks and present a spectral analysis of spiking and local field potential activity recorded in the cortex from two macaques during a memory-saccade task . Their results indicate dynamic memory fields in neuronal activity that are specific to both the direction and time of a planned movement. We show their (population-average) spike spectrum recorded during the working-memory task in Panel 2D and the spectrum of a representative single cell in Panel 2E. The spectra are well-aligned with our proposed filter in Panel 2C, suggesting that frequency usage in important cognitive functions might be proportional to their robustness against common types of spike-train anomalies.

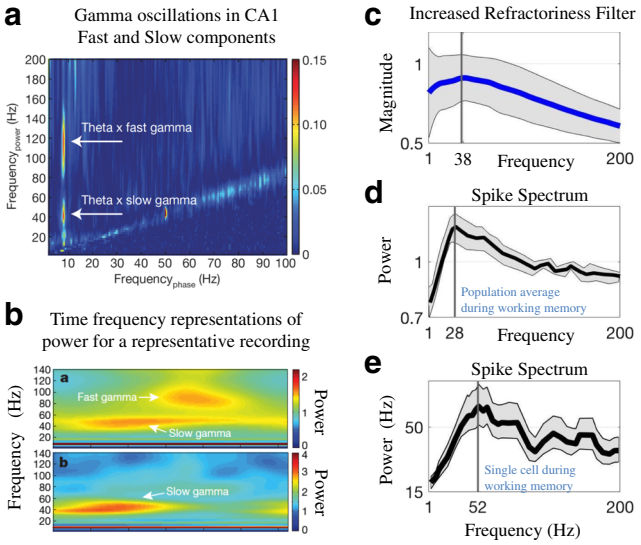

Fig. 2 Consequences of slow-gamma robustness for memory retrieval. **a** Cross-frequency coherence plot from Colgin et al. (2009) shows two separate bands (fast ≈ 65–140 Hz and slow ≈ 25–50 Hz) of gamma power (y-axis) modulated by the theta phase (x-axis) in the CA1 are of the hippocampus. **b** Time frequency representation of power for a representative CA1 cell recording, also adapted from Colgin et al. (2009). We hypothesize that slow-gamma ranges near 40Hz are involved in memory retrieval due to its robustness against common types of spike-train anomalies. **c** Plot shows the (normalized) magnitude of each transmitted frequency (in Hz) for increased refractoriness impairment type. We annotate the most robust frequency (37 Hz), and remark that the slow-gamma range lies in the vicinity of this maximal value. Conversely, fast gamma frequencies are more vulnerable to such effects. **d–e** Population average and single-cell spike spectrum recorded in the cortex of two macaques during a working memory task from Pesaran et al. (2002). The spectra from Panels D–E are well aligned with the filer in Panel C, suggesting that frequency usage in important cognitive functions might be proportional to their robustness against injurious mechanisms

3 Discussion

A common practice in computational neuroscience is to model neuronal pathologies in a binary way, by treating a neuron and/or its connections as either fully functional or fully impaired. Recent developments show, however, that these simpler strategies are not able to capture the experimentally observed frequency-dependent errors in spike-train propagation that arise in leading brain disorders. Our phenomenological signal-processing framework accounts for major cellular-level pathologies that distort spike train propagation, including axonal swellings and demyelination. In fact, robustness-to-injury might justify why the brain advantageously exploits the slow gamma range in a broad array of cognitive functions.

Model compatibility with TBI experiments in rats Our proposed pile up impairment mechanism seems to agree with recent rat experiments with induced mild Traumatic Brain

Injury (mTBI). Munyon et al. (2014) investigated changes in hippocampal firing rate patterns during a novel object recognition task in rats after mTBI. They concluded that memory deficits after mTBI are associated with lower intrinsic bursting activity and impaired context-specific firing patterns in the hippocampus during object exploration. More specifically, they reported that spike trains after TBI had significantly lower intra-burst spike frequencies. In fact, the raster plots for cells in the hippocampus of a sham rat exhibit several tightly consecutive spikes, but these pairs are rare in the recordings following TBI. While it is not clear if the observed changes in spike-trains are due to individual neural impairments or due to different collective network deficits, our hypothesis is plausible as pile-up effects delete proximal spikes, which in turn, increases the ISI within bursts.

Impaired TC for visual and motor experiments Tuning Curves (TC) are widely employed to characterize neuronal responses to stimuli. Since our increased refractoriness filter is frequency-dependent, we can estimate impaired TC and potential encoding errors for a few classic experiments: (i) neural responses of the visual cortex as a bar of light moves across the receptive field at different angles (Dayan and Abbot 2001; Henry et al. 1974; Hubel and Wiesel 1968; Wandell 1995), (ii) retinal disparity recordings for a cat V1 neuron (Dayan and Abbot 2001; Poggio and Talbot 1981; Wandell 1995), and (iii) recordings from a neuron in the primary motor cortex of a monkey during an arm-reaching task (Dayan and Abbot 2001; Georgopoulos et al. 1982). The mismatch between healthy and impaired TCs might help identify potential encoding and decoding errors in the information processing stages in of the task. In all cases, our results provide testable hypothesis for future experiments. See the Methods section for details.

MRF always in the 38–41 Hz range Regardless of our parameter choices, the bode-plots for our increased refractoriness filters have always the same qualitative shape, with a most robust frequency in the 38–41Hz range. This may be justified by a Goldilocks-type of argument: spike deletion (via pile-up) rarely occurs in trains generated by a low firing-rate Poisson process. When they do, however, the third spike in line is typically so far from the transmitted first spike that it leads to a drastic (local) increase in the inter-spike interval (ISI). This, in turn, leads to a sharp (local) decrease in frequency. At intermediate frequencies (30–45 Hz), pile up occurs more often, but the ISI does not increase so much, and thus, one effect balances the other. Finally, at higher frequencies, pile-ups become so frequent that they overcompensate for their smaller impact on ISI. As a consequence, frequencies in the 38-41 Hz range (slow-gamma range) seem to be optimally guarded, in a statistical sense, against this common type of injury. See the SI for a detailed discussion on how such results hold for a broad range of parameter and kernel choices.

3.1 Special role of neural-responses in the 40-Hz frequency range

The brain seems to take advantage of the robustness of slow-gamma frequencies (near 40 Hz) in a broad array of cognitive functions. As recently summarized in Saleem et al. (2017), gamma rhythms (30-90 Hz) occur in a wide range of brain circuits including the amygdala, cerebellum, cortex, hippocampus, and others (Fries 2009; Middleton et al. 2008; Cardin et al. 2009; Sohal et al. 2009). They are commonly implicated in functions such as information transmission between distinct neuronal subpopulations (Fries 2005; 2009), perception (Fries et al. 2007), attentional selection (Fries et al. 2001) and memory (Montgomery and Buzsaki 2007). We discuss a few instances in more detail below.

Special role of 40-Hz in memory The CA1 area of the hippocampus is known to split its gamma oscillations in two distinct components: a fast band ($\approx$ 90 Hz) and slow band ($\approx$ 40 Hz). See Colgin et al. (2016, 2009) for details. The hippocampus plays a critical role in memory (Squire et al. 2004), and there, the authors suggest that the fast gamma frequencies facilitate memory encoding while the slow gamma components are involved in memory retrieval. This separation is important to reliably distinguish the perceptions of ongoing experiences from the internally evoked memories. It is therefore intriguing that our model's MRF lies within 38-41 Hz, while higher frequencies were severely compromised (see Fig. 2). This could explain, for instance, why patients with common neurological conditions can retrieve older stored memories more effectively (action that involves slow gamma) than can create new ones (involves high gamma). This is the case in TBI-induced memory impairment (Christodoulou et al. 2001), in Alzheimer's disease (Kirk and Berntsen 2017) and in the kinds of cognitive dysfunction seen in Multiple Sclerosis (Rao et al. 1989; Rocca et al. 2015).

Special role of 40-Hz in attenuating AD symptoms Changes in slow-gamma oscillations have been observed in several neurological disorders, but most prominently in rat models for Alzheimer's Disease (AD) (Palop et al. 2007; Verret et al. 2012). Iaccarino et al. (2016) showed that external stimulation of CA1 neurons meticulously at 40 Hz attenuates the formation of A-beta proteins and plaque associated with AD in mice. While our calculations do not explain the histological improvements following the treatment, they suggest that 40 Hz stimulation may provide

an unexpected but beneficial collateral effect at a signal-transmission-level: if more neurons lock/synchronize at more robust frequencies, the overall capability of the system to transmit information may also improve. A potential clinical implication of this is that emerging brain stimulation treatments like transcranial magnetic stimulation and direct current stimulation might have optimal efficacy when applied in the slow gamma range.

Special role of 40-Hz in visual consciousness and awareness Gold (1999) argued that synchronous oscillations at this value are causally implicated in visual consciousness. Several studies of phase-locking in neural oscillations followed the report of 40-Hz synchronous activity in the visual cortex of a cat by Gray et al. (1989), and led F. Crick and C. Koch to make the 40-Hz oscillation the centerpiece of their theory of visual consciousness and awareness (Crick and Koch 1990a, b, 1992; Koch and Crick 1994). They further postulated that objects for which the binding problem has been solved are placed into working memory (Crick and Koch 1990b), and this idea was later confirmed by reports of peaks near 40 Hz in the power spectrum of dynamic memory fields in working memory tasks (Pesaran et al. 2002). It is not clear, however, why this specific value is used. This work suggests a compelling hypothesis, namely, that the brain advantageously exploit the robustness of slow-gamma frequencies at a cellular level to transmit information in a more reliable way.

Limitations The output of a given neuron ultimately depends on the entire network in which the cell is embedded. Thus, when we propose a filter for an injured cell, we are modeling signal distortions that occur at an individual level. In other words, our filters do *not* capture collective network malfunction and should be regarded as building blocks for modeling impaired networks. This disambiguation is important since gamma rhythms at a population level are largely associated with the collective inhibition caused by interneurons. Perhaps the most straightforward way to experimentally validate our filters is to grow and damage neurons *in vitro*, record the (same) spike train before and after the axonal injury location, and check if our proposed i/o rules are a good proxy for the observed signal distortion. At this point, we make no connections between our proposed filters and physiological implications to cells that produce the gamma rhythm or to the inputs to those cells from other parts of the cortex.

While our results highlight impairments that increase refractoriness in spike trains, there are many other modes of failures (see Section 2.1). Frequencies optimally guarded against them may vary. Our filters were derived from simulations involving Poisson spike trains and are yet to be validated on empirical datasets. The variability of inter-spike intervals (ISI) are of fundamental importance for some types of neuronal impairments. Since different spike-generating processes lead to different distributions of ISI, some processes can be more exposed (or robust) to injuries than the ones we tested. The optimality of the slow-gamma frequencies must also be regarded in a statistical sense, i.e., it focuses on steady-state frequency responses and ignores transient effects that might be relevant in modeling cascades and synchrony in neural circuits. Finally, the degree of injury was not considered in the present results, and it will likely depend on individual cases as frequency response in human subjects may vary.

Future directions Healthy synchronous activity of large neuronal populations are well understood in all classic frequency bands. See Rapp et al. (2015) for a recent review, and in particular, their summary of changes in spectral power associated with mild traumatic brain injuries. We remark that the majority of spectral studies listed by them, however, involve only lower frequencies (delta, theta, alpha), while studies involving the gamma band are still largely open. With such a diverse range of frequency bands, neuronal circuits, and functionalities, our results may help guide electrophysiological experiments as to what frequencies are more endangered and/or robust in different pathological scenarios.

4 Methods

4.1 Basic definitions, terminology and notation

Throughout this work, we model a spiking neuron as a discrete-time system responding to a time-dependent stimulus $s(t)$. The neuronal response consists of a discrete sequence of binary values $\{x_n\} = [x_0, x_1, \ldots, x_N]$, recorded at times $\{t_n\} = [t_0, t_1, \ldots, t_N]$, according to some input/output rule F:

$$\underbrace{s(t)}_{\text{stimulus}} \xrightarrow{F} \underbrace{[x_0, x_1, \ldots, x_N]}_{\text{spike train response}}$$

The rule given by F can be sophisticated: it can be nonlinear, have a stochastic component, depend on several state variables (like the Hodgkin-Huxley model), depend on the combined input from neighboring neurons, etc. Unless stated otherwise, we assume that the recorded times are equally spaced, i.e., that $|t_{i+1} - t_i| = \triangle t$ for all i, and that no more than a single spike is counted within $\triangle t$. For simplicity, we will consider spikes as identical stereotypical

events and ignore differences in their duration, amplitude, and shape. Thus, we have:

$$x_i = \begin{cases} 1 \text{ if a spike was elicited between } (t_{i-1}, t_i], \\ 0 \text{ otherwise.} \end{cases}$$

Intuitively, a *spike-train* $\{x_n\}$ is a sequence (or vector) made of zeros and ones with enough resolution to produce the raster plots commonly observed throughout the neuroscience literature. There are different mathematical formulations to model spike trains (see for instance (Dayan and Abbot 2001; Reich et al. 1998; Rieke et al. 1995)), but our setup is particularly convenient to describe a large variety of impairments caused by neuronal pathologies. We represent each *type* of impairments by a mathematical/computational rule. For instance, a *total blocking* impairment is a rule to delete all spikes within a spike train:

$$[x_0, x_1, \ldots, x_n] \to [0, 0, \ldots, 0] \text{ or } y_n = 0 \cdot x_n.$$

4.2 List of i/o rules for neuronal impairments

Our list of input/output rules for neuronal impairments follows closely the schematic representation of the conduction properties of {normal vs demyelinated axons} or {before vs after FAS} from Fig. 1b–c. Thus, the output (injured) train y_n is obtained by applying a mathematical rule to the input (healthy) train x_n. See the Results section for details.

4.3 Generating healthy Poisson spike trains

Our i/o rules for neuronal impairments can be applied generically to any spike train, but it is important in applications to generate input (healthy) spike trains that are compatible with the neuronal activity in question. In what follows, we will generate spike trains via a Poisson Process (PP) of intensity (or firing-rate) λ, i.e., when the inter-spike interval τ is governed by a memoryless exponential random variable of the form $P[\tau] = \lambda \exp(-\lambda\tau)$. We summarize the statistical properties of Poisson spike trains in Table 1. This choice is somewhat pedagogical (see Dayan and Abbot (2001) and Rieke et al. (1995)), and we acknowledge that there are other important processes to generate spike trains such as modulated and resampled PP, leaky and non-leaky integrate-and-fire, modulated gamma processes, and others that cannot be well approximated by the simpler PP (see Reich et al. (1998)).

The statistical properties of the input spike trains, and more specifically, the variability of inter-spike intervals (ISI) are of fundamental importance for some types of neuronal impairments. For example, the increasing refractoriness rule deletes the second spike whenever the ISI of a consecutive pair is sufficiently close. Since different spike-generating processes lead to different distributions of ISI, some processes can be more exposed (or robust) to this type injury than the PP. In fact, from a robustness-to-injury perspective, not all firing-rates are created equal: if two spike-generating processes have the same average firing-rate frequency but different ISI distributions, the one with higher ISI will be more robust to this type of injury than the other. We conjecture that this feature may play an important role in information encoding, especially along long axonal tracts.

Table 1 Properties for poisson process with firing rate λ

Symbol	Equation	Remarks
$P_T[n]$	$= \frac{(\lambda T)^n}{n!} \exp(-\lambda T)$	*Prob. of n spikes within T*
$\langle n \rangle$	$= \lambda T$	*Average number of spikes*
σ_n^2	$= \lambda T$	*Variance in spike count*
ISI	$= \lvert\tilde{t}_{i+1} - \tilde{t}_i\rvert$	*Inter-Spike Interval*
$P[\tau]$	$= \lambda \exp(-\lambda\tau)$	*Exponential distribution*
$\langle \tau \rangle$	$= 1/\lambda$	*Mean of the ISI*
σ_τ^2	$= 1/\lambda^2$	*Variance of the ISI*
C_V	$= \sigma_\tau / \langle\tau\rangle$	*Coefficient of variation*

4.4 Approximating firing rates from spike trains

As discussed in Dayan and Abbot (2001), the firing rate cannot be determined exactly from a limited number of spike train responses. As a consequence, there are different methods to approximate/infer this quantity, with the simplest one consisting in discretizing time into bins of duration $\triangle t$, counting the number of spikes within each bin, and dividing by $\triangle t$. See Figs. 3 and 4 for examples of this bin-and-count procedure applied to a healthy spike train (in black) and to its distorted counterpart after injury (in red). To mitigate the biases created by the arbitrary bin placement, it is customary to slide a kernel window function $w(\tau)$ along the spike train ρ and approximate the firing rate r continuously:

$$r(t) \approx \int_{-\infty}^{+\infty} w(\tau)\rho(t-\tau)d\tau \tag{9}$$

Table 2 lists commonly used kernels, and Figs. 3 and 4 illustrate their different firing-rate approximations for the same spike train example. Unless stated otherwise, we will

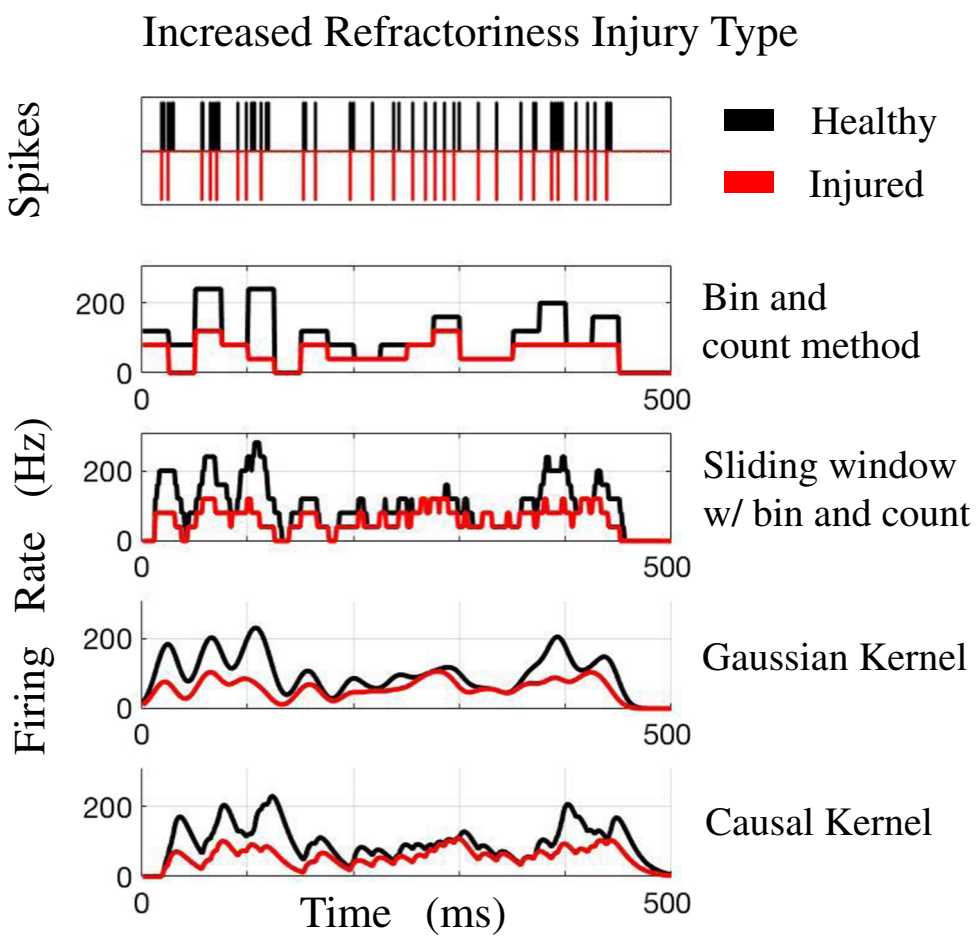

Fig. 3 Effects of increased refractoriness to spike trains and neuronal firing rates. In this commonly-observed type of impairment (also referred to as filtering or pile-up effect (Maia and Kutz 2014a)), if two consecutive spikes are sufficiently close, the second spike will be deleted and only the first one will propagate. This occurs in demyelination (see Fig. 1c and Smith (1994)) and in focal axonal swellings (see Fig. 1d and Maia et al. (2015) and Maia and Kutz (2017)). The top plot exemplifies a healthy Poisson spike train (in black) and the corresponding injured spike train (in red). Notice that the refractory period of the neural response is effectively increased. See Eq. (5) for the precise mathematical rule applied to the healthy train to obtain the injured one. Additional plots approximate the firing rates of both spike trains by convolving them with commonly used kernels. See Table 2. We will also estimate continuous counterparts for the discrete-time filters to show how different frequencies are affected by the injury. See text for details

use the *Causal kernel* as default, in which the temporal resolution is given by $1/\alpha$.

4.5 Estimating continuous transfer functions for impairments

Our set of discrete-time filters provides a rich framework to model how spike trains are transformed in impaired tracts. Since firing-rate neural networks are still widely used in computational simulations of brain circuits, it is natural to extend our filters continuously to firing-rates as well. For this, we follow the script below:

1. Generate spike trains compatible with the normal/healthy neural responses. Select the impairment type from our i/o list along with plausible parameters.
2. Approximate firing rates from spike trains before and after injury by convolving them with a suitable kernel (see Table 2). Healthy and injured responses are now measured as frequency (typically in Hz) over time (typically in ms). See Figs. 3–4 for some examples.
3. Track how a fixed frequency in the input/healthy signal is transformed into others in the corresponding output/injured signal. Do this for all pairs, over all times, for all frequencies.
4. Summarize the results into a frequency-dependent continuous filter that can be applied to any healthy signal to obtain its (average) injured counterpart.
5. Obtain Bode plots for the continuous filters depicting changes in magnitude (typically in dB) and in phase (typically in degrees).

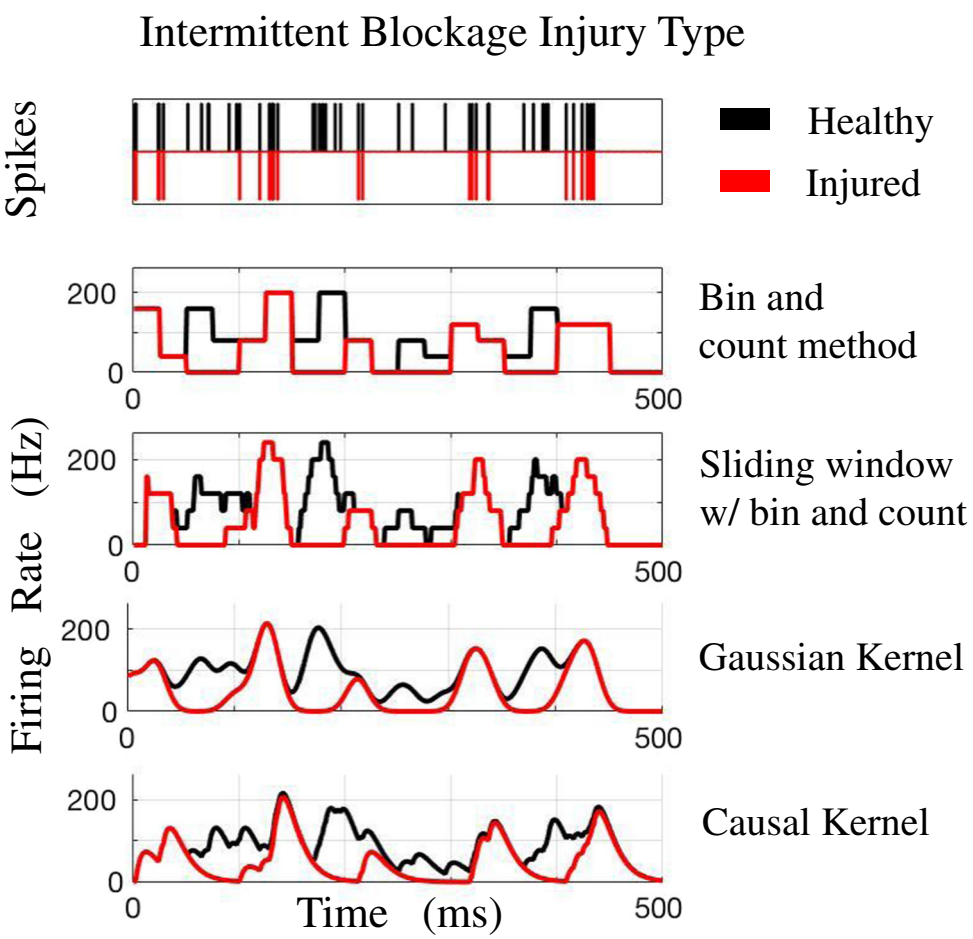

Fig. 4 Effects of intermittent blockage to spike trains and neuronal firing rates. This type of impairment was reported in demyelinated axons (see Fig. 1c and Smith (1994)). Top plot exemplifies a healthy Poisson spike train (in black) and the corresponding injured spike train (in red). Notice that injured spike train exhibit periodic windows of no firing activity. See Eq. (7) for the precise mathematical rule applied to the healthy train to obtain the injured one. Additional plots approximate the firing rates of both spike trains by convolving them with commonly used kernels. See Table 2. We will also estimate continuous counterparts for the discrete-time filters to show how different frequencies are affected by the injury. See text or details

There are two sensible approaches for estimating the transfer function (steps 3-5). In the first, one could use Welch's spectral density estimator to determine the marginal and joint spectra. This requires making a choice of which estimator type (their H1 or H2), as well as the parameters for the Welch's estimator (the window type, the size of a window, the amount of overlap, etc.). Finally, it would also need a statistical procedure to determine the parameter values for the spectral density estimator (Fan and Kreutzberger 1998). Alternatively, one could use the raw periodogram and cross-periodogram per each trial, and then average those over trials. We use the second procedure to get unbiased estimates of the true spectra and average across trials to reduce the variability of the estimates.

Figure 1 shows filters for increased refractoriness impairment for different kernels and parameters. The filters in Fig. 5 correspond to the intermittent blockage impairment (with switching frequency $\omega = \pi/50$) and to the evoked potentials impairment. They can be interpreted as continuous-filter counterparts for the i/o rules in Eqs. (7) and (8) respectively. Their bode plots are significantly different from increased refractoriness impairment, with Fig. 5a exhibiting an accentuated phase shift and with the magnitude values in Fig. 5b being positive for all frequencies.

Table 2 Commonly used kernels (window functions) to convolve with observed spike trains to obtain approximate Firing Rates (FR):

Name	Equation
Bin and Count[1]	$w(t) = \begin{cases} 1/\triangle t & \text{if } -\frac{\triangle t}{2} \le t \le \frac{\triangle t}{2} \\ 0 & \text{otherwise.} \end{cases}$
Gaussian Kernel[2]	$w(\tau) = \frac{1}{\sqrt{2\pi\sigma_w}} \exp\left(\frac{-\tau^2}{2\sigma_w}\right)$
Causal Kernel[3]	$w(\tau) = [\alpha^2 \exp(-\alpha\tau)]_+$

[1]Uses bins of length $\triangle t$ to control the temporal resolution

[2]Where σ_w controls the temporal resolution

[3]Where $1/\alpha$ controls the temporal resolution

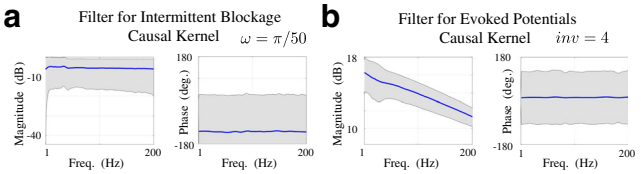

Fig. 5 Bode plots for continuous filters corresponding to other types of neural impairments. **a** Filter for intermittent blockage with switching frequency $\omega = \pi/50$. As expected, there was a significant shift in the average phase plot. See Eq. (7) and text for details. **b** Filter for evoked potentials, where in this case, a input spike triggers 4 others. Notice that the magnitude values are positive for all frequencies. See Eq. (8) and text for details. In all cases, the input spike trains were realization of a Poisson process, and one should expect different values for the filters if other methods are used instead

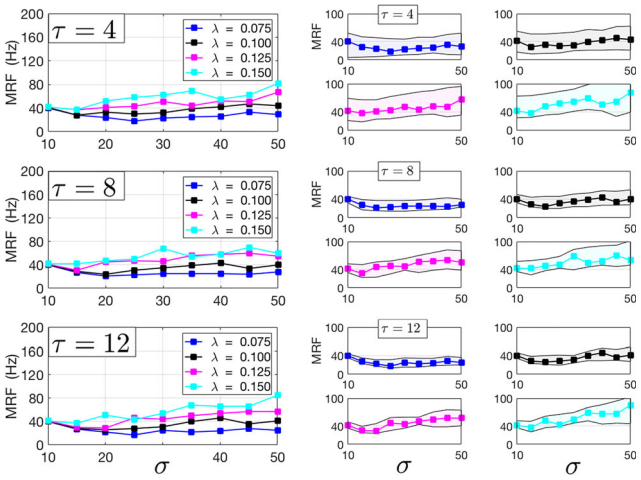

Fig. 6 Robustness of results to parameter choices. We estimate the Most Robust Frequency (MRF) to the increased-refractoriness injury for different values of: Poisson spike-generator intensity (λ = 0.075, 0.100, 0.125 and 0.150 spikes/millisecond), for different sizes of kernel window (σ = 10, 15, 20, ..., and 50 ms), and for different refractoriness parameters (τ = 4, 8 and 12ms). The large panels on the left depict the MRF as a function of and . Every point annotated in the graphs was averaged over 3000 spike trains of length 1000ms each. Thus, the figure summarizes simulations. Note that for $\sigma = 10$ all plots give MRF = 40 Hz. The smaller panels on the right show a zoomed version of the larger panels on the left. Denoting m^* the magnitude (amplitude) associated with the MRF, we shade frequencies with magnitude above $.95m^*$. Larger λ, τ, and σ values lead to larger MRF, but slow-gamma frequencies always remain within the MRF band

4.6 Robustness of results to parameter choices

A crucial aspect of our results is its robustness to broad changes in parameters. There are two parameters involved in generating (healthy) response-frequencies: the intensity of the Poisson spike-generator and the kernel window-size used during the convolution step. We remark that the same frequency (in Hz) can have different underlying statistics of Inter-Spike-Intervals (ISI) that in turn, can be convolved with kernels of different resolution. The ISI depends on λ and the Firing Rate (FR) depends on σ. Low values (high values) of σ correspond to a high resolution (low resolution) Gaussian kernel. Thus, a FR = 100 Hz generated by $\lambda = 0.100$ spikes/millisecond and $\sigma = 10ms$ has a different underlying spike-train structure than a FR = 100 Hz generated by $\lambda = 0.125$ spikes/millisecond and $\sigma = 50ms$. It is reasonable to expect that the Most Robust Frequency (MRF) to injury would also depend on λ and/or σ. Figure 6 summarizes an extensive parameter space exploration to show that, for a broad range of parameter values, the MRF remains within the slow-gamma frequency band (5-fold increase in σ, 1.5-fold increase and .75-fold decrease in λ, and 3-fold increase in τ) (Fig. 6).

4.7 Spike train input generated by non-Homogeneous Poisson Processes (nHPP)

Our results thus far focused on input spike trains being generated by a Homogeneous Poisson Process. However, given the high dependency of the transfer function to the input process, we investigate if our main result still holds in a more biologically plausible scenario. It is expected that a neuron responding to a stimulus will generate spike trains that are better approximated by non-Homogeneous Poisson Processes (nHPP), i.e., when the intensity λ of the process is now time-dependent $\lambda(t)$. It is customary in neuroscience to model $\lambda(t)$ with a piecewise-constant function (see Dayan and Abbot (2001)), and thus, we will follow the schematics for $\lambda(t)$ shown in Fig. 7a: (i) we assume that the neuron has a lower baseline firing rate given by λ_{base}. (ii) At $t = t_1$, the intensity increases to an intermediate value λ_{int} triggered by some stimulus. (iii) At $t = t_2$, the intensity achieves its maximum value λ_{max}. (iv) Finally, at $t = t_3$, the stimulus ends and λ drops to its baseline value. In our nHPP simulations, we will treat a spike train generated by steps (i)-(iv) as one input realization and proceed as before to obtain the corresponding filters. In what follows we will show that changes in the duration and in the intensity of each step (i)-(iv) do not affect the MRF.

As schematized in Fig. 7a, we scale the maximum intensity λ_{max} by multiplying it by different values of α, and set $\lambda_{base} = \lambda_{max}/4$ and $\lambda_{int} = \lambda_{max}/2$. Analogously, we fix the duration $\triangle t$ of steps (i), (ii) and (iv) and scale the length of step (iii) by multiplying it with β for different values of β. The range for both scaling factors α and β consists of [0.50, 0.75, 1.00, 1.25, 1.50, 1.75]. Figure 7b shows amplitude (magnitude) filters for $\lambda_{max} = .100$ spikes/millisecond, with $\triangle t = 200ms$, for the increasing refractoriness injury type ($\tau = 4$ms), for extremal values of

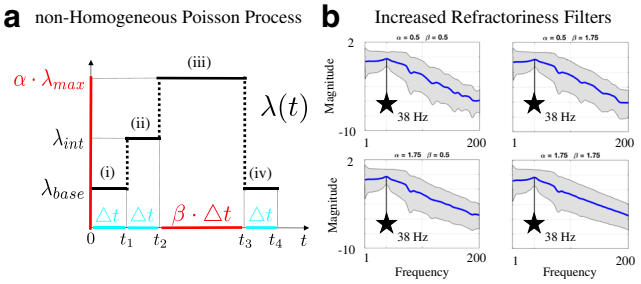

Fig. 7 Robustness of results to non-Homogeneous Poisson Process (nHPP). **a** To model a more biologically plausible time-dependent $\lambda(t)$, we assume that (i) the neuron has a lower baseline firing rate given by λ_{base}, (ii) at $t = t_1$, the intensity increases to an intermediate value λ_{int} triggered by some stimulus, (iii) at $t = t_2$, the intensity achieves its maximum value λ_{max}, and (iv) at $t = t_3$, the stimulus ends and λ drops to its baseline value. We vary the intensity and duration of step (iii) by multiplying λ_{max} and $\triangle t$ by α and β in [0.50, 0.75, 1.00, 1.25, 1.50, 1.75]. **b** shows amplitude (magnitude) filters for the increasing refractoriness injury type ($\tau = 4$ms) for [$\alpha = .50, \beta = .50$], [$\alpha = .50, \beta = 1.75$], [$\alpha = 1.75, \beta = .50$], and [$\alpha = 1.75, \beta = 1.75$]. Note that there are no significant changes to the transfer function and that MRF = 38 Hz holds for all cases, suggesting that the robustness of slow-gamma may hold for multiple models of spike train statistics

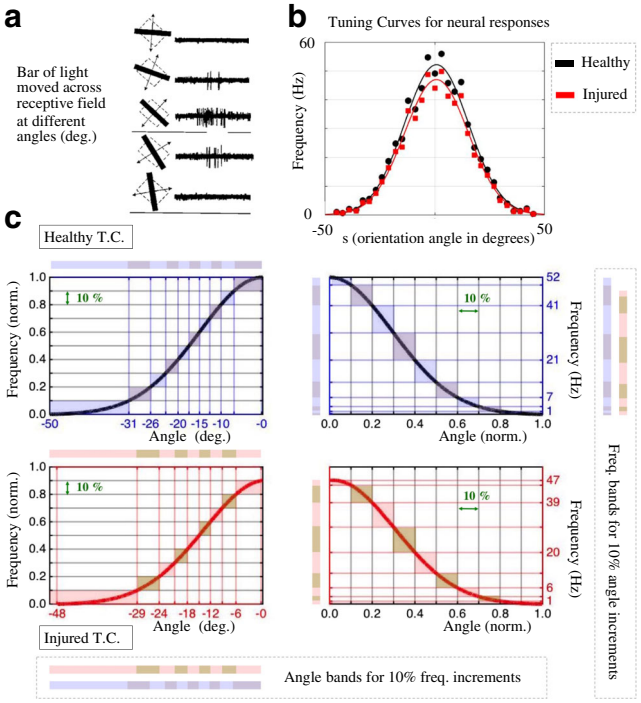

Fig. 8 **a** Recordings from a neuron in the primary visual cortex of a monkey. A bar of light was moved across the receptive field of the cell at different angles, adapted from Dayan and Abbot (2001), Wandell (Wandell 1995) and Hubel and Wiesel (1968). **b** Average firing rate (in Hz) of a cat V1 neuron plotted in black as a function of the orientation angle of the light bar stimulus, adapted from Dayan and Abbot (2001) and Henry et al. (1974). Estimated injured/filtered response (in red) for neuron with increased refractoriness impairment. **c** Detailed comparison between healthy and injured Tuning Curves (T.C.); notice the changes in angular bands for 10% frequency increments (left plots) and the changes in frequency bands for 10% angular increments (right plots). These discrepancies in signal encoding and decoding may lead to confusion and errors in the neural information processing stages

α and β in the range above. Note that there are no significant changes to the overall shape of the transfer function, and that the MRF remains the same in all cases. The invariance of the MRF (around 38 Hz) to piecewise-constant nHPPs is a strong indicator that the robustness of the slow-gamma range may hold for multiple neuronal models of spike train statistics.

4.8 Impaired TC for visual and motor experiments

Tuning Curves (TC) are widely employed to characterize neuronal responses to stimuli. As shown in Dayan and Abbot (2001), the firing rate (frequency) - derived from the number of action potentials fired during several trials of the task - is typically written as a function of an appropriate stimulus parameter. Since our increased refractoriness injury filter is frequency-dependent (see Fig. 1), we can estimate corresponding impaired TC and potential encoding errors for a few classic experiments.

Impaired TC in visual experiments Figure 8a is adapted from Dayan and Abbot (2001) and shows extracellular recordings from the primary visual cortex of a monkey as a bar of light moves across the receptive field of the cell at different angles (Hubel and Wiesel 1968; Wandell 1995). Figure 8b plots a TC (in black) for analogous experiments done on a cat (Henry et al. 1974). We apply the increased refractoriness filter (Fig. 1) to the healthy TC to estimate its injurious counterpart (in red). Panel 5C compares both curves in details; we annotate grids with 10% increments in the frequency response range (y-axis) and the corresponding angle bands they encode (x-axis). This lead to the horizontal bars (on the bottom) with alternating light and dark colors (blue for healthy TC and red for injured TC). Analogously, we annotate the grids on the right plots with 10% increments in the angle range (x-axis) and their corresponding frequency bands (y-axis), which yields the vertical bars (on the right). The mismatch between bars might help identify potential encoding and decoding errors in the information processing stages of the task.

Figure 9 shows a second example of impaired tuning curve for a visual-experiment, also following Dayan and Abbot (2001). Figure 9a schematizes the notion of retinal disparity, where the position of an object located nearer than the fixation point in the retina is shifted. Figure 9b shows the healthy TC (in black) for a cat V1 neuron responding (in freq.) to separate bars of light illuminating each eye as a function of the retinal disparity (stimulus).

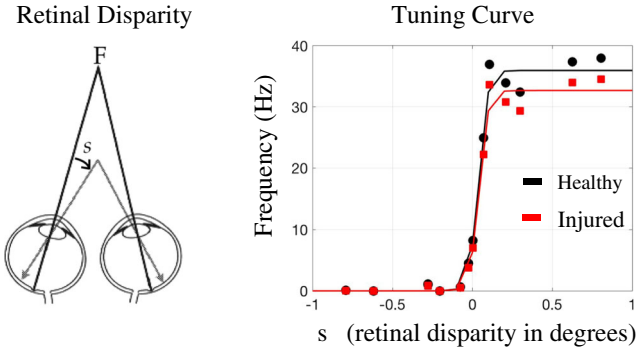

Fig. 9 **a** Definition of retinal disparity (adapted from Dayan and Abbot (2001) and Wandell (1995)), where arrows show the location on each retina of an object located nearer than the fixation point F. The disparity angle s is also indicated. **b** Average firing rate of a cat V1 neuron responding to separate bars of light illuminating each eye as a function of the disparity angle. The healthy tuning curve is plot in black and adapted from Dayan and Abbot (2001) and Poggio and Talbot (1981). The estimated injured/filtered response is shown in red for a neuron with increased refractoriness impairment. See text for more details

The corresponding injured TC is shown in red. Once again, higher frequencies are more affected by the pathological mechanism than slower frequencies and may lead to more encoding/decoding errors.

Impaired TC in motor experiments Our last TC example applies to a brain area in which the neural responses represent a motor action. Figure 10a (adapted from Dayan and Abbot (2001) and Georgopoulos et al. (1982)) depicts recordings from a neuron in the primary motor cortex of a monkey during an arm-reaching task. In this setup, the neuronal response frequency f varies according to the reaching angle s of the arm movement. Figure 10b shows the healthy TC in black (adapted from Dayan and Abbot (2001) and Georgopoulos et al. (1982)) and the corresponding injured TC in red (for the increased refractoriness impairment). In Fig. 10c, we annotate the grids with 10% increments as before. One can easily see the discrepancies between the healthy and injured incremental bands for decoding (horizontal bars) and encoding (vertical bars). Most interestingly, the results show that the angular directions between $100° - 225°$ (i.e., in the third quadrant in Fig. 10a) exhibit the highest discrepancies between healthy vs injured TCs. Thus, we conjecture that a monkey with neuronal impairments to the M1 caused by traumatic brain injuries (and/or other brain disorders) would experience accentuated motor difficulties in reaching these specific directions. Conversely, the monkey would perform significantly better when reaching directions associated with low frequencies ($0° - 90°$ and $270° - 360°$). This provides a mathematically precise, intuitive and *testable* hypothesis for future experiments to validate our models.

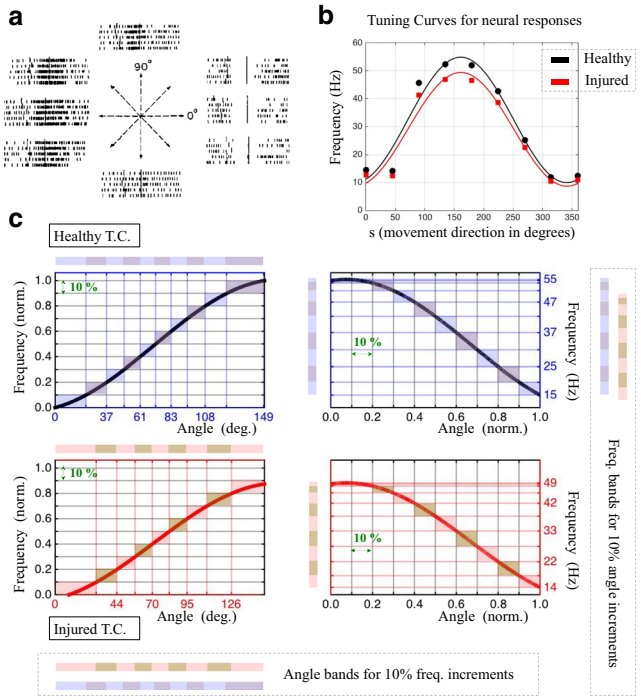

Fig. 10 **a** Recordings from the primary motor cortex of a monkey performing an arm-reaching task. Rasters for different reaching directions show action potentials fired on five trials. Figure adapted from Dayan and Abbot (2001) and Georgopoulos et al. (1982). **b** Average firing rate plotted as a function of the direction in which the monkey moved its arm. Healthy tuning curve (TC), plot in black, was also adapted from Dayan and Abbot (2001) and Georgopoulos et al. (1982), while the red injured TC was estimated for a neuron with increased refractoriness impairment. See text for more details. **c** Detailed comparison between healthy and injured TCs; notice the changes in angular bands for 10% frequency increments (left plots) and the changes in frequency bands for 10% angular increments (right plots). The angular directions between $100° - 225°$ (i.e., in the third quadrant in Panel A) exhibit the highest discrepancies. Thus, we conjecture that a monkey with neuronal impairments to the M1 caused by traumatic brain injuries (and/or other brain disorders) would experience accentuated motor difficulties in reaching these directions. Conversely, the monkey would perform significantly better when reaching directions associated with low frequencies ($0° - 90°$ and $270° - 360°$). This provides a precise and testable hypothesis for future experiments

5 Summary

Injured neurons distort, confuse or block the information encoded in spike trains. Wether injury occurs through demyelinating effects or focal axonal swellings, spike trains are compromised in a similar fashion in traumatic brain injuries as well as a number of leading neurodegenerative diseases such as Alzheimers and Multiple Sclerosis. These incurable brain disorders are of great societal interest since they are respectively the most common type of autoimmune disease, dementia, and a leading source of death/disability among youngsters. We show in a simple phenomenological

model of single cells that neural-response frequencies in the slow-gamma range of 38–41 Hz statistically emerge as the most insulated against common spike-train distortions caused by injury. Since external stimulation at precisely 40 Hz ameliorated Alzheimer's symptoms in a recent mice experiment, the slow-gamma robustness at a cellular level may provide an unexpected beneficial side effect to signal transmission as well. Our findings may also help explain why this band is so strongly implicated in both memory retrieval and visual consciousness.

References

Adalbert, R., Nogradi, A., Babetto, E., Janeckova, L., Walker, S.A., Kerschensteiner, M., Misgeld, T., Coleman, M.P. (2009). Severely dystrophic axons at amyloid plaques remain continuous and connected to viable cell bodies. *BRAIN*, *132*, 402–416.

Adams, J.H., Jennett, B., Murray, L.S., Teasdale, G.M., Gennarelli, T.A., Graham, D.I. (2011). Neuropathological findings in disabled survivors of a head injury. *Journal of Neurotrauma*, *28*, 701–709.

Browne, K.D., Chen, X.H., Meaney, D.F., Smith DH (2011). Mild traumatic brain injury and diffuse axonal injury in swine. *Journal of Neurotrauma*, *28*(9), 1747–1755.

Browne, K.D., Chen, X.H., Meaney, D.F. (2011). Smith DH Mild traumatic brain injury and diffuse axonal injury in swine. *Journal of Neurotrauma*, *28*(9), 1747–1755.

Cardin, J.A., Carlen, M., Meletis, K., Knoblich, U., Zhang, F., Deisseroth, K., Tsai, L.H., Moore, C.I. (2009). Driving fast-spiking cells induces gamma rhythm and controls sensory responses. *Nature*, *459*, 663–667.

Colgin, L.L. (2016). Rhythms of the hippocampal network. *Nature Reviews Neuroscience*, *17*, 239–249.

Colgin, L.L., Denninger, T., Fyhn, M., Hafting, T., Bonnevie, T., Jensen, O., Moser, M.B., Moser, E.I. (2009). Frequency of gamma oscillations routes flow of information in the hippocampus. *Nature*, *462*, 353–357.

Crick, F., & Koch, C. (1990). Some reflections on visual awareness. *Cold Spring Harbor Symposia on Quantitative Biology*, *55*, 953–962.

Crick, F., & Koch, C. (1990). Towards a neurobiological theory of consciousness. *Seminars in the Neurosciences*, *2*, 263–275.

Crick, F., & Koch, C. (1992). The problem of consciousness. *Scientific American*, *26*, 153–159.

Christodoulou, C., DeLuca, J., Ricker, J.H., Madigan, N.K., Bly, B.M., Lange, G., Kalnin, A.J., Liu, W.C., Steffener, J., Diamond, B.J., Ni, A.C. (2001). Functional magnetic resonance imaging of working memory impairment after traumatic brain injury Journal of Neurology. *Neurosurgery & Psychiatry*, *71*(2), 161–168.

Daianu, M., Jacobs, R.E., Town, T., Thompson, P.M. (2016). Axonal diameter and density estimated with 7-tesla hybrid diffusion imaging in transgenic alzheimer rats. *SPIE Proceedings*, *9784*, 1–6.

Dayan, P., & Abbot, L.F. (2001). *Theoretical neuroscience*. Cambridge: MIT Press.

De Stefano, N., Matthews, P.M., Antel, J.P., Preul, M., Francis, G., Arnold, D.L. (1995). Chemical pathology of acute demyelinating lesions and its correlation with disability. *Annals of Neurology*, *38*(6), 901–909.

Dikranian, K., Cohen, R., Donald, C.M., Pan, Y., Brakefield, D., Bayly, P., Parsadanian, A. (2008). Mild traumatic brain injury to the infant mouse causes robust white matter axonal degeneration which precedes apoptotic death of cortical and thalamic neurons. *Experimental Neurology*, *211*, 551–560.

Edlow, B.L., Copen, W.A., Izzy, S., van der Kouwe, A., Glenn, M.B., Greenberg, S.M., Greer, D.M., Wu, O. (2016). Longitudinal diffusion tensor imaging detects recovery of fractional anisotropy within traumatic axonal injury lesions. *Neurocritical Care*, *24*(3), 342–352.

Fan, J., & Kreutzberger, E. (1998). Automatic local smoothing for spectral density estimation. *Scandinavian Journal of Statistics*, *25*(2), 359–369.

Fries, P. (2005). A mechanism for cognitive dynamics: neuronal communication through neuronal coherence. *Trends in Cognitive Sciences*, *9*, 474–480.

Fries, P. (2009). Neuronal gamma-band synchronization as a fundamental process in cortical computation. *Annual Reviews in Neuroscience*, *32*, 209–224.

Fries, P., Nikolic, D., Singer, W. (2007). The gamma cycle. *Trends in Neuroscience*, *30*, 309–316.

Fries, P., Reynolds, J.H., Rorie, A.E., Desimone, R. (2001). Modulation of oscillatory neuronal synchronization by selective visual attention. *Science*, *29*, 1560–1563.

Friese, M.A., Schattling, B., Fugger, L. (2014). Mechanisms of neurodegeneration and axonal dysfunction in multiple sclerosis. *Nature Reviews Neurology*, *10*, 225–238.

Georgopoulos, A.P., Kalaska, J.F., Caminiti, R., Massey, J.T. (1982). On the relations between the directions of two-dimensional arm movements and cell discharge in primate motor cortex. *Journal of Neuroscience*, *2*, 1527–1537.

Gold, I. (1999). Does 40-Hz oscillation play a role in visual consciousness *Consciousness and Cognition*, *8*, 186–195.

Gray, C.M., Konig, P., Engel, A.K., Singer, W. (1989). Oscillatory responses in cat visual cortex exhibit inter-columnar synchronization which reflects global stimulus properties. *Nature*, *338*, 334–337.

Hanell, A., Greer, J.E., McGinn, M.J., Povlishock, J.T. (2015). Traumatic brain injury-induced axonal phenotypes react differently to treatment. *Acta Neuropathologica*, *129*, 317–332.

Hellman, A.N., Vahidi, B., Kim, H.J., Mismar, W., Steward, O., Jeonde, N.L., Venugopalan, V. (2010). Examination of axonal injury and regeneration in micropatterned neuronal culture using pulsed laser microbeam dissection. Lab on a Chip; 16.

Henry, G.H., Dreher, B., Bishop, P.O. (1974). Orientation specificity of cells in cat striate cortex. *Journal of Neurophysiology*, *37*, 1394–1409.

Hemphill, M., Dauth, S., Yu, C.J., Dabiri, B., Parker, K. (2015). Traumatic brain injury and the neuronal microenvironment: a potential role for neuropathological mechanotransduction. *Neuron*, *86*(6), 1177–1192.

Henninger, N., Bouley, J., Sikoglu, E.M., An, J., Moore, C.M., King, J.A., Bowser, R., Freeman, M.R., Brown, R.H. Jr. (2016). Attenuated traumatic axonal injury and improved functional outcome after traumatic brain injury in mice lacking sarm1. *BRAIN*, *139*, 1–12.

Herwerth, M., Kalluri, S.R., Srivastava, R., Kleele, T., Kenet, S., Illes, Z., Merkler, D., Bennett, J.L., Misgeld, T., Hemmer, B. (2016). In vivo imaging reveals rapid astrocyte depletion and axon damage in a model of neuromyelitis optica-related pathology. *Annals of Neurology*, *79*, 794–805.

Hill, C.S., Coleman, M.P., Menon, D.K. (2016). Traumatic axonal injury: mechanisms and translational opportunities. *Trends in Neuroscience*, *39*(5), 311–324.

Hubel, D.H., & Wiesel, T.N. (1968). Receptive fields and functional architecture of the monkey striate cortex. *Journal of Physiology*, *195*, 215–243.

Iaccarino, H.F., Singer, A.C., Martorell, A.J., Rudenko, A., Gao, F., Gillingham, T.Z., Mathys, H., Seo, J., Kritskiy, O., Abdurrob, F., Adaikkan, C., Canter, R.G., Rueda, R., Brown, E.N., Boyden, E.S., Tsai, L.H. (2016). Gamma frequency entrainment attenuates amyloid load and modifies microglia. *Nature*, *540*, 230–235.

Johnson, V.E., Stewart, W., Smith, D.H. (2013). Axonal pathology in traumatic brain injury. *Experimental Neurology*, *246*, 35–43.

Jorge, R.E., Acion, L., White, T., Tordesillas-Gutierrez, D., Pierson, R., Crespo-Facorro, B., Magnotta, V. (2012). White matter abnormalities in veterans with mild traumatic brain injury. *American Journal of Psychiatry*, *169*(12), 1284–1291.

Karlsson, P., Haroutounian, S., Polydefkis, M., Nyengaard, J.R., Jensen, T.S. (2016). Structural and functional characterization of nerve fibres in polyneuropathy and healthy subjects. *Scandinavian Journal of Pain*, *10*, 28–35.

Kirk, M., & Berntsen, D. (2017). A short cut to the past: cueing via concrete objects improves autobiographical memory retrieval in Alzheimer's disease patients. Neuropsychologia; issn 0028–3932.

Koch, C., & Crick, F. (1994). *Some further ideas regarding the neuronal basis of awareness. Large-scale neuronal theories of the brain*. Cambridge: MIT.

Kolaric, K.V., Thomson, G., Edgar, J.M., Brown, A.M. (2013). Focal axonal swellings and associated ultrastructural changes attenuate conduction velocity in central nervous system axons: a computer modeling study. *Physiological Reports*, *1*(3), e00,059.

Kornek, B., Storch, M.K., Weissert, R., Wallstroem, E., Stefferl, A., Olsson, T., Linington, C., Schmidbauer, M., Lassmann, H. (2000). Multiple sclerosis and chronic autoimmune encephalomyelitis. *The American Journal of Pathology*, *157*, 267–276.

Krstic, D., & Knuesel, I. (2012). Deciphering the mechanism underlying late-onset Alzheimer disease. *Nature Reviews Neuroscience*, *9*(1), 25–34.

Lachance, M., Longtin, A., Morris, C.E., Yu, N., Joos, B. (2014). Stimulation-induced ectopicity and propagation windows in model damaged axons. *Journal of Computational Neuroscience*, *37*, 523–531.

Laukka, J.J., Kamholz, J., Bessert, D. (2016). Novel pathologic findings in patients with pelizaeus-merzbacher disease. Neuroscience Letters.

Louis, E.D., Faust, P.L., Vonsattel, J., Honig, L.S., Rajput, A., Pahwa, R., Lyons, K.E., Ross, G.W., Elble, R.J., Erickson-Davis, C., Moskowitz, C.B., Lawton, A. (2009). Torpedoes in parkinson?s disease, alzheimer's disease, essential tremor, and control brains. *Movement Disorders*, *24*(11), 1600–1605.

Magdesian, M.H., Sanchez, F., Lopez, M., Thostrup, P., Durisic, N., Belkaid, W., Liazoghli, D., Grütter, P., Colman, R. (2012). Atomic force microscopy reveals important differences in axonal resistance to injury. *Biophysical Journal*, *103*(3), 405–414.

Maia, P.D., & Kutz, J.N. (2017). Reaction time impairments in decision-making networks as a diagnostic marker for traumatic brain injury and neurodegenerative diseases. *Journal of Computational Neuroscience*, *42*(3), 323–347.

Maia, P.D., Hemphill, M.A., Zehnder, B., Zhang, C., Parker, K.K., Kutz, J.N. (2015). Diagnostic tools for evaluating the impact of Focal Axonal Swellings arising in neurodegenerative diseases and/or traumatic brain injury. *Journal of Neuroscience Methods*, *253*, 233–243.

Maia, P.D., & Kutz, J.N. (2014). Compromised axonal functionality after neurodegeneration, concussion and/or traumatic brain injury. *Journal of Computational Neuroscience*, *27*, 317–332.

Maia, P.D., & Kutz, J.N. (2014). Identifying critical regions for spike propagation in axon segments. *Journal of Computational Neuroscience*, *36*(2), 141–155.

Middleton, S.J., Racca, C., Cunningham, M.O., Traub, R.D., Monyer, H., Knopfel, T., Schofield, I.S., Jenkins, A., Whittington, M.A. (2008). High-frequency network oscillations in cerebellar cortex. *Neuron*, *58*, 763–774.

Montgomery, S.M., & Buzsaki, G. (2007). Gamma oscillations dynamically couple hippocampal CA3 and CA1 regions during memory task performance. *Proceeding of National Academy of Science*, *104*, 14495–14500.

Morrison, B., Elkin, B.S., Dolle, J.P., Yarmush, M.L. (2011). In vitro models of traumatic brain injury. *Annual Reviews in Biomedical Engineering*, *13*(1), 91–126.

Munyon, C., Eakin, K.C., Sweet, J.A., Miller, J.P. (2014). Decreased bursting and novel object-specific cell firing in the hippocampus after mild traumatic brain injury. *Brain Research*, *1582*, 220–226.

Nikic, I., Merkler, D., Sorbara, C., Brinkoetter, M., Kreutzfeld, M., Bareyre, F., Bruck, W., Bishop, D., Misgeld, T., Kerschensteiner, M. (2011). A reversible form of axon damage in experimental autoimmune encephalomyelitis and multiple sclerosis. *Nature Medicine*, *17*(4), 495–499.

Palop, J.J., Chin, J., Roberson1, E.D., Wang, J., Thwin, M.T., Bien-Ly, N., Yoo, J., Ho, K.O., Yu, G.Q., Kreitzer, A., Finkbeiner, S., Noebels, J.L., Mucke, L. (2007). Aberrant excitatory neuronal activity and compensatory remodeling of inhibitory hippocampal circuits in mouse models of Alzheimer's disease. *Neuron*, *55*, 697–711.

Pesaran, B., Pezaris, J.S., Sahani, M., Mitra, P.P., Andersen, R.A. (2002). Temporal structure in neuronal activity during working memory in macaque parietal cortex. *Nature Neuroscience*, *5*(8), 805–811.

Poggio, G.F., & Talbot, W.H. (1981). Mechanisms of static and dynamic stereopsis in foveal cortex of the rhesus monkey. *Journal of Physiology*, *315*, 469–492.

Rao, S.M., Leo, G.J., Haughton, V.M., St Aubin-Faubert, P., Bernardin, L. (1989). Correlation of magnetic resonance imaging with neuropsychological testing in multiple sclerosis. *Neurology*, *39*, 161–66.

Rapp, P.E., Keyser, D.O., Albano, A., Hernandez, R., Gibson, D.B., Zambon, R.A., Hairston, W.D., Hughes, J.D., Krystal, A., Nichols, A.S. (2015). Traumatic brain injury detection using electrophysiological methods. *Frontiers in Human Neuroscience*, *9*(11), 1–32.

Reeves, T.M., Smith, T.L., Williamson, J.C., Phillips, L.L. (2012). Unmyelinated axons show selective rostrocaudal pathology in the corpus callosum after traumatic brain injury. *Journal of Neuropathology & Experimental Neurology*, *71*(3), 198–210.

Reich, D.S., Victor, J.D., Knight, B.W. (1998). The power ration and the interval map: spiking models and extracellular recordings. *The Journal of Neuroscience*, *18*(23), 10090–100104.

Rieke, F.M., Warland, D., van Steveninck, R.R., Bialek, W. (1995). *Spikes: exploring the neural code*. Cambridge: MIT Press.

Rocca, M.A., Amato, M.P., De Stefano, N., Enzinger, C., Geurts, J.J., Penner, I.K., Rovira, A., Sumowski, J.F., Valsasina, P., Filippi, M. (2015). Clinical and imaging assessment of cognitive dysfunction in multiple sclerosis. *The Lancet Neurology*, *14*(3), 302–317.

Rudy, S., Maia, P.D., Kutz, J.N. (2016). Cognitive and behavioral deficits arising from neurodegeneration and traumatic brain injury: a model for the underlying role of focal axonal swellings in neuronal networks with plasticity. Journal of Systems and Integrative Neuroscience.

Saleem, A.B., Lien, A.D., Krumin, M., Haider, B., Roson, M.R., Ayaz, A., Reinhold, K., Busse, L., Carandini, M., Harris, K.D. (2017). Subcortical source and modulation of the narrowband gamma oscillation in mouse visual cortex. *Neuron*, *93*, 315–322.

Sharp, D.J., Scott, G., Leech, R. (2014). Network dysfunction after traumatic brain injury. *Nature Reviews Neurology*, *10*, 156–166.

Sohal, V.S., Zhang, F., Yizhar, O., Deisseroth, K. (2009). Parvalbumin neurons and gamma rhythms enhance cortical circuit performance. *Nature*, *459*, 698–702.

Smith, K.J. (1994). Conduction properties of central demyelinated and remyelinated axons, and their relation to symptom production in demyelinating disorders. *Eye*, *8*, 224–237.

Squire, L.R., Stark, C.E., Clark, R.E. (2004). The medial temporal lobe. *Annual Reviews in Neuroscience*, *27*, 279–306.

Tagliaferro, P., & Burke, R.E. (2016). Retrograde axonal degeneration in parkinson disease. *Journal of Parkinson's Disease*, *6*, 1–15.

Tang-Schomer, M.D., Johnson, V.E., Baas, P.W., Stewart, W., Smith, D.H. (2012). Partial interruption of axonal transport due to microtubule breakage accounts for the formation of periodic varicosities after traumatic axonal injury. *Experimental Neurology*, *233*, 364–372.

Tang-Schomer, M.D., Patel, A., Bass, P.W., Smith, D.H. (2010). Mechanical breaking of microtubules in axons during dynamic stretch injury underlies delayed elasticity, microtubule disassembly, and axon degeneration. *The FASEB Journal*, *24*(5), 1401–1410.

Trapp, B.D., & Nave, K.A. (2008). Multiple sclerosis: An immune or neurodegenerative disorder *Annual Review Neuroscience*, *31*(1), 247–269.

Trapp, B.D., Peterson, J.W., Ransohoff, R.M., Rudick, R.A., Mork, S., Bo, L., Mork, S., Bo, L. (1998). Axonal transection in the lesions of multiple sclerosis. *The New England Journal of Medicine*, *338*, 278–285.

Verden, D., & Macklin, W.B. (2016). Neuroprotection by central nervous system remyelination: molecular, cellular, and functional considerations. *Journal of Neuroscience Research*, *94*, 1411–1420.

Verret, L., Mann, E.O., Hang, G.B., Barth, A.M.I., Cobos, I., Ho, K., Devidze, N., Masliah, E., Kreitzer, A.C., Mody, I., Mucke, L., Palop, J.J. (2012). Inhibitory interneuron deficit links altered network activity and cognitive dysfunction in Alzheimer model. *Cell*, *149*, 708–721.

Wandell, B.A. (1995). Foundations of vision Sunderland, MA: Sinauer Assciates.

Wang, J., Hamm, R.J., Povlishock, J.T. (2011). Traumatic axonal injury in the optic nerve: evidence for axonal swelling, disconnection, dieback and reorganization. *Journal of Neurotrauma*, *28*(7), 1185–1198.

Waxman, S.G. (2006). Axonal conduction and injury in multiple sclerosis: the role of sodium channels. *Nature Reviews Neuroscience*, *7*, 932–941.

Zlochiver, S. (2010). Persistent reflection underlies ectopic activity in multiple sclerosis: a numerical study. *Biological Cybernnetics*, *102*, 181–196.